

Higgs boson pair production in the little Higgs model at hadron colliders *

Liu Jing-Jing², Ma Wen-Gan^{1,2}, Li Gang², Zhang Ren-You² and Hou Hong-Sheng²

¹ CCAST (World Laboratory), P.O.Box 8730, Beijing 100080, P.R.China

² Department of Modern Physics, University of Science and Technology
of China (USTC), Hefei, Anhui 230027, P.R.China

Abstract

The Higgs boson pair production process at hadron collider provides an opportunity for performing a study of the trilinear Higgs boson self-coupling. In this paper, we analyze the pair production of a neutral Higgs boson via both gluon-gluon and $b\bar{b}$ fusions in the littlest Higgs (LH) model at the CERN LHC. We find that in some parameter space the relative corrections of the total cross section to the SM prediction may reach a value of 24% when $x (= 4fv'/v^2) = 0.95$ at the LHC. We conclude that if the parameter x has a value above 0.8, the relative corrections contributed by the LH model reach values beyond 8% and can be observed at the LHC.

PACS: 12.60.Cn, 13.85.Fb, 14.80.Bn

*Supported by National Natural Science Foundation of China.

1 Introduction

The standard model(SM) [1, 2] theory has been proved by all existing precise experimental data with its theoretical predictions beyond one-loop level being coincident with experimental observations. But in the SM the Higgs boson mass suffers from an instability under radiative corrections. This "hierarchy problem" motivates much of current research works about new physics beyond the SM. Among the extended models beyond the SM, the little Higgs model offers a very promising solution to the hierarchy problem in which the Higgs boson is naturally light as a result of nonlinearly realized symmetry [3]-[8]. The first successful model, which cancels all relevant quadratic divergences based on the pseudo Goldstone idea, was constructed by Arkani-Hamed, Cohen, and Georgi [3]. Then more models were constructed, such as $SU(5)/SO(5)$ [6], $SU(6)/SP(6)$ [7], and the minimal moose $SU(3)^2/SU(3)$ [5] and general moose $SU(3)^n/SU(3)^k$ [9]. The most economical model of them is the littlest Higgs (LH) model, which is based on an $SU(5)/SO(5)$ non-linear sigma model [6]. It consists of a $SU(5)$ global symmetry, which is spontaneously broken down to $SO(5)$ by a vacuum condensate f . In the LH model, a set of new heavy gauge bosons (A_H, Z_H, W_H) and a new heavy-vector-like quark (T) are introduced which just cancel the quadratic divergence induced by SM gauge boson loops and the top quark loop, respectively.

One of the most important task of present and future experiments is to search for Higgs boson and investigate its properties. Studying the properties of the Higgs potential will reveal details of mass-generation mechanism in spontaneously broken gauge theories, which can be obtained through measuring the Higgs boson self-interactions. Multiple Higgs

boson production processes at hadron colliders provide the way to probe the Higgs boson self-interactions. Many works have been contributed to studies of Higgs-pair production at the hadron collider in some traditional models [10]-[13]. The possibility of measuring the Higgs boson self-coupling at the LHC has been investigated by U. Baur, T. Plehn and D. Rainwater [14]. They found that it should be possible at the CERN Large Hadron Collider (LHC) with design luminosity to establish that the SM Higgs boson has nonzero self-coupling and that λ/λ_{SM} can be restricted to a range of $0 - 3.7$ at 95% confidence level if its mass is between 150 to 200 GeV. Recently, the LH model contribution to the Higgs decay width was investigated in Refs. [15] and [16]. Dib *et al.*, discussed also the LH model contribution to the process $pp \rightarrow H^0 H^0 + X$ in Ref. [15]. There they did not consider mixing and interference effects between the SM particles and the new heavy states, and thus they got negligible results of the order of $(v/f)^4$ and concluded that the contribution from the LH model to the pair production to the Higgs bosons seems to be unobservable at the LHC [15]. If the interference and mixing effects are included in the analysis, the contribution is at the order $(v/f)^2$ and does change obviously the results as compared to the SM prediction in some parameter space [16].

In this paper we investigate the effect of the LH model on neutral Higgs boson pair production via both gluon and bottom fusions at the CERN Large Hadron Collider (i.e., $gg \rightarrow H^0 H^0$ and $b\bar{b} \rightarrow H^0 H^0$) at the complete lowest order, considering mixing and interference effects between the SM particles and the new heavy states. The paper is organized as follows. In Sec. 2, we briefly go through the LH model theory. In Sec. 3, we present an analytical evaluation. The numerical results, discussion and a short summary

are given in Sec. 4. Finally we present the relevant Feynman rules in the Appendix.

2 littlest Higgs model

The littlest Higgs model is based on an $SU(5)/SO(5)$ nonlinear sigma model. At the scale $\Lambda_s \sim 4\pi f$, the vacuum expectation value (VEV) associated with the spontaneous symmetry breaking proportional to the scale f is parameterized by the 5×5 symmetry matrix [6] [17]

$$\Sigma_0 = \begin{pmatrix} & & \mathbf{1}_{2 \times 2} \\ & 1 & \\ \mathbf{1}_{2 \times 2} & & \end{pmatrix}. \quad (1)$$

The VEV breaks the $SU(5)$ global symmetry into its subgroup $SO(5)$ and breaks the local gauge symmetry $[SU(2) \otimes U(1)]^2$ into its diagonal subgroup $SU(2)_L \otimes U(1)_Y$ at the same time, which is identified as the SM electroweak gauge group. The scalar fields are parameterized by

$$\Sigma(x) = e^{i\Pi(x)/f} \Sigma_0 e^{i\Pi(x)^T/f}, \quad (2)$$

where $\Pi(x) = \pi^a(x)X^a$ is the Goldstone boson matrix. X^a are the broken generators of $SU(5)$ which obey the relation

$$X^a \Sigma_0 - \Sigma_0 X^{aT} = 0. \quad (3)$$

Therefore, the Goldstone boson matrix $\Pi(x)$ can be expressed as

$$\Pi = \begin{pmatrix} & h^\dagger/\sqrt{2} & \phi^\dagger \\ h/\sqrt{2} & & h^*/\sqrt{2} \\ \phi & h^T/\sqrt{2} & \end{pmatrix}, \quad (4)$$

where

$$h = \begin{pmatrix} h^+ & h^0 \end{pmatrix}, \quad \phi = \begin{pmatrix} \phi^{++} & \phi^+/\sqrt{2} \\ \phi^+/\sqrt{2} & \phi^0 \end{pmatrix} \quad (5)$$

are a doublet and triplet under the unbroken $SU(2)_L \otimes U(1)_Y$ SM gauge group, respectively.

The leading-order dimension-2 term for the scalar fields $\Sigma(x)$ in the littlest Higgs model can be written as

$$\mathcal{L} = \frac{1}{2} \frac{f^2}{4} \text{Tr} |\mathcal{D}_\mu \Sigma|^2. \quad (6)$$

\mathcal{D}_μ is the covariant derivative for gauge group $[SU(2) \otimes U(1)]^2 = [SU(2)_1 \otimes U(1)_1] \otimes [SU(2)_2 \otimes U(1)_2]$. It is defined as

$$\mathcal{D}_\mu \Sigma = \partial_\mu \Sigma - i \sum_{j=1}^2 [g_j (W_j \Sigma + \Sigma W_j^T) + g'_j (B_j \Sigma + \Sigma B_j^T)], \quad (7)$$

where $W_{\mu j} = \sum_{a=1}^3 W_{\mu j}^a Q_j^a$ and $B_j = B_{\mu j} Y_j$ are the $SU(2)_j$ and $U(1)_j$ gauge fields, respectively. The generators of two $SU(2)$'s (Q_j^a) and two $U(1)$'s generators (Y_j) are as follows

$$Q_1^a = \begin{pmatrix} \frac{\sigma^a}{2} & \\ & \mathbf{0}_{3 \times 3} \end{pmatrix}, \quad Q_2^a = \begin{pmatrix} \mathbf{0}_{3 \times 3} & \\ & -\frac{\sigma^{a*}}{2} \end{pmatrix},$$

$$Y_1 = \text{diag}\{-3, -3, 2, 2, 2\}/10, \quad Y_2 = \text{diag}\{-2, -2, -2, 3, 3\}/10, \quad (8)$$

where σ^a ($a = 1, 2, 3$) are the Pauli matrices. As we expect, the breaking of the gauge symmetry $[SU(2) \times U(1)]^2$ into its diagonal subgroup $SU(2)_L \times U(1)_Y$ gives rise to heavy gauge bosons W' and B' , and the remaining unbroken subgroup $SU(2)_L \times U(1)_Y$ introduces the massless gauge bosons W and B .

As we know, in the littlest Higgs model there is no Higgs potential at the tree level. Instead, the Higgs potential is generated at one loop and higher orders due to the interactions with gauge bosons and fermions. Up to operators of dimension 4, the Higgs potential (Coleman-Weinberg potential) can be expressed as [16] [17]

$$V = \lambda_{\phi^2} f^2 \text{Tr}(\phi^\dagger \phi) + i \lambda_{h\phi h} f (h \phi^\dagger h^T - h^* \phi h^\dagger) - \mu^2 h h^\dagger + \lambda_{h^4} (h h^\dagger)^2$$

$$+\lambda_{h\phi\phi h}h\phi^\dagger\phi h^\dagger + \lambda_{h^2\phi^2}hh^\dagger\text{Tr}(\phi^\dagger\phi) + \lambda_{\phi^2\phi^2}\left[\text{Tr}(\phi^\dagger\phi)\right]^2 + \lambda_{\phi^4}\text{Tr}(\phi^\dagger\phi\phi^\dagger\phi), \quad (9)$$

where λ_{ϕ^2} , $\lambda_{h\phi h}$, λ_{h^4} , $\lambda_{h\phi\phi h}$, $\lambda_{h^2\phi^2}$, $\lambda_{\phi^2\phi^2}$, and λ_{ϕ^4} are the coefficients of the original Higgs potential. The coefficients which are concerned in our calculation have the expressions as [16]

$$\lambda_{\phi^2} = \frac{M_\phi^2}{f^2}, \quad \lambda_{h\phi h} = \frac{xM_\phi^2}{2f^2}, \quad \lambda_{h^4} = \frac{M_\phi^2}{4f^2}, \quad \lambda_{h\phi\phi h} = -\frac{4M_\phi^2}{3f^2}. \quad (10)$$

By minimizing the Coleman-Weinberg potential, we obtain the vacuum expectation values $\langle h^0 \rangle = v/\sqrt{2}$, $\langle i\phi^0 \rangle = v'$ of the Higgs boson doublet h and triplet ϕ , which give rise to electroweak symmetry breaking (EWSB). The Coleman-Weinberg potential provides the trilinear and quartic Higgs self-couplings. After EWSB, the gauge sector gets an additional mass and mixing term due to the VEVs of h and ϕ . By diagonalizing the quadratic term of the gauge sector, we may get the mass eigenstates A_L , Z_L , W_L , A_H , Z_H , and W_H and their masses.

To avoid large quadratic divergence in the Higgs boson mass due to the heavy top quark Yukawa interaction, we introduce a pair of new fermions \tilde{t} and \tilde{t}' [6] [17] and a set of new interactions. The scalar couplings to the top quark can be taken from the following Lagrangian [6] [17]:

$$\mathcal{L}_Y = \frac{1}{2}\lambda_1 f \epsilon_{ijk} \epsilon_{xy} \chi_i \Sigma_{jx} \Sigma_{ky} u_3^c + \lambda_2 f \tilde{t} \tilde{t}'^c + H.C. \quad (11)$$

where $\chi = (b_3, t_3, \tilde{t})$, ϵ_{ijk} and ϵ_{xy} are antisymmetric tensors where i, j, k run through 1, 2, 3 and x, y run through 4, 5, and λ_1 and λ_2 are the new model parameters. By expanding the above Lagrangian, we get the physical states of the top quark t and a new

heavy-vector-like quark T . The masses of the two physical states are

$$m_t = \frac{v\lambda_1\lambda_2}{\sqrt{\lambda_1^2 + \lambda_2^2}} \left\{ 1 + \frac{v^2}{f^2} \left[-\frac{1}{3} + \frac{fv'}{v^2} + \frac{1}{2} \frac{\lambda_1^2}{\lambda_1^2 + \lambda_2^2} \left(1 - \frac{\lambda_1^2}{\lambda_1^2 + \lambda_2^2} \right) \right] \right\}, \quad (12)$$

$$m_T = f\sqrt{\lambda_1^2 + \lambda_2^2} [1 + \mathcal{O}(v^2/f^2)], \quad (13)$$

respectively. Since the top quark mass is already obtained in the SM, we can then get the parameter relation from Eq. (12) as deduced in Ref. [17]

$$\frac{1}{\lambda_1^2} + \frac{1}{\lambda_2^2} \approx \frac{v^2}{m_t^2} \approx 2. \quad (14)$$

3 Calculation

At hadron collider, the Higgs boson pair can be produced through two mechanisms. One is loop-induced production via gluon fusion; the other is from $b\bar{b}$ annihilation. The Feynman diagrams contributing to the subprocess $gg \rightarrow H^0 H^0$, which are involved in the framework of the LH model, are depicted in Fig. 1. The diagrams created by exchanging two external gluon lines and final Higgs boson lines are not shown there. In Fig. 1, the first three diagrams (Fig. 1(1)-1(3)) [excluding the Fig. 1(1) with a heavy- vector-like quark (T) loop] are just the same as those in the framework of the SM, while the remaining four figures (Fig. 1(4)-1(7)) are the extra diagrams beyond the SM. All the Feynman diagrams can be classified into three types. The first type is named as s -channel diagrams with the exchange of a virtual neutral Higgs boson H^0 or heavy triplet Higgs boson Φ^0 which couples to a pair of gluons via a triangle quark loop [shown in Fig.1(1), 1(4)]. The second type is called box diagrams [shown in Fig. 1(2), 1(3), 1(5), 1(6)] and the third is the

quartic interaction type where the neutral Higgs bosons are produced by means of quartic interactions [shown in Fig. 1(7)]. All the relevant Feynman rules can be found in Ref. [17] and the Appendix in this paper. In the loop diagram calculation of this subprocess, we adopt a dimensional regularization scheme. The Feynman diagrams for the subprocess $b\bar{b} \rightarrow H^0 H^0$ are depicted in Fig. 2. In this work we adopted the Feynman-'t Hooft gauge.

In our calculation, we denote the two subprocesses as

$$g(c_1, p_1) + g(c_2, p_2) \rightarrow H^0(k_1) + H^0(k_2), \quad (15)$$

$$b(c_3, p_1) + \bar{b}(c_4, p_2) \rightarrow H^0(k_1) + H^0(k_2). \quad (16)$$

where c_1, c_2, c_3 , and c_4 are the color indexes of the two initial particles (gg and $b\bar{b}$). p_1, p_2 and k_1, k_2 are the incoming and outgoing four-momenta of the initial and final particles, respectively. In the subprocess $gg \rightarrow H^0 H^0$, we define θ as the scattering angle between one of the gluons and one of the final H^0 bosons, and in the subprocess $b\bar{b} \rightarrow H^0 H^0$, θ represents the scattering angle between the b quark and one of the final Higgs bosons. In the center-of-mass system (c.m.s.) the four-momenta of the initial and final particles can be expressed as ¹

$$\begin{aligned} p_1 &= \left(\frac{\sqrt{\hat{s}}}{2}, 0, 0, \frac{\sqrt{\hat{s}}}{2} \right), \\ p_2 &= \left(\frac{\sqrt{\hat{s}}}{2}, 0, 0, -\frac{\sqrt{\hat{s}}}{2} \right), \\ k_1 &= \left(\frac{\sqrt{\hat{s}}}{2}, \frac{\sqrt{\hat{s}}}{2}\beta_{H^0} \sin \theta, 0, \frac{\sqrt{\hat{s}}}{2}\beta_{H^0} \cos \theta \right), \\ k_2 &= \left(\frac{\sqrt{\hat{s}}}{2}, -\frac{\sqrt{\hat{s}}}{2}\beta_{H^0} \sin \theta, 0, -\frac{\sqrt{\hat{s}}}{2}\beta_{H^0} \cos \theta \right), \end{aligned} \quad (17)$$

¹In our calculation we set the mass of the b quark to be zero except in the Yukawa coupling.

where $\beta_{H^0} = \sqrt{1 - 4m_{H^0}^2/\hat{s}}$ is the velocity of final neutral Higgs bosons in the c.m.s. and $\hat{s} = (p_1 + p_2)^2$.

The amplitude for the subprocess $gg \rightarrow H^0 H^0$ can be expressed as

$$\begin{aligned} \mathcal{M}(gg \rightarrow H^0 H^0) &= \mathcal{M}^{(t)} + \mathcal{M}^{(b)} + \mathcal{M}^{(q)} \\ &= \epsilon_\mu(p_1) \epsilon_\nu(p_2) \left(f_1 g^{\mu\nu} \delta_{c_1 c_2} + f_2 k_1^\mu k_1^\nu \delta_{c_1 c_2} + f_3 \epsilon^{\alpha\mu\nu\beta} k_{1\alpha} p_{1\beta} \right. \\ &\quad \left. + f_4 \epsilon^{\alpha\mu\nu\beta} k_{1\alpha} p_{2\beta} + f_5 \epsilon^{\mu\nu\alpha\beta} p_{1\alpha} p_{2\beta} \right), \end{aligned} \quad (18)$$

where $\mathcal{M}^{(t)}$, $\mathcal{M}^{(b)}$, and $\mathcal{M}^{(q)}$ represent the amplitudes of triangle, box, and quartic diagrams, respectively.

For the subprocess $b\bar{b} \rightarrow H^0 H^0$, the amplitude can be expressed as

$$\mathcal{M}(b\bar{b} \rightarrow H^0 H^0) = \bar{v}(p_2) (g_1 + g_2 \not{k}_1) \delta_{c_3 c_4} u(p_1). \quad (19)$$

In the above two equations f_i ($i = 1, \dots, 5$) and g_j ($j = 1, 2$) are the form factors of the two subprocesses, respectively. Since the explicit expressions of these form factors are lengthy, we do not list them in this paper.²

Then the total cross sections for these two subprocesses can be written as

$$\hat{\sigma}(\hat{s}, gg \rightarrow H^0 H^0) = \frac{1}{32\pi\hat{s}^2} \int_{\hat{t}^-}^{\hat{t}^+} d\hat{t} \overline{\sum} |\mathcal{M}(gg \rightarrow H^0 H^0)|^2, \quad (20)$$

$$\hat{\sigma}(\hat{s}, b\bar{b} \rightarrow H^0 H^0) = \frac{1}{32\pi\hat{s}^2} \int_{\hat{t}^-}^{\hat{t}^+} d\hat{t} \overline{\sum} |\mathcal{M}(b\bar{b} \rightarrow H^0 H^0)|^2, \quad (21)$$

respectively, where the bar over the summation recalls averaging over initial spins and colors, $\hat{t}^\pm = (m_{H^0}^2 - \hat{s}/2 \pm \hat{s}\beta_{H^0}/2)$, and due to the identical final two Higgs bosons, the

²The Mathematica program codes of all the form factors for $gg \rightarrow H^0 H^0$ and $b\bar{b} \rightarrow H^0 H^0$ are obtainable by sending an email to moonbank@mail.ustc.edu.cn

right-hand sides of Eqs. (20) and (21) have been multiplied by an additional factor of 1/2 separately. The color and spin average factors for the subprocess $gg \rightarrow H^0 H^0$ are 1/64 and 1/4 and for the subprocess $b\bar{b} \rightarrow H^0 H^0$ are 1/9 and 1/4, respectively. The total cross section for the neutral Higgs boson pair production through gluon (or bottom) fusion in proton-proton collisions can be obtained by performing the following integration

$$\sigma(pp \rightarrow gg(b\bar{b}) \rightarrow H^0 H^0) = \int_{4m_{H^0}^2/s}^1 d\tau \frac{dL_{ij}}{d\tau} \hat{\sigma}(\hat{s} = \tau s, gg(b\bar{b}) \rightarrow H^0 H^0), \quad (22)$$

where \sqrt{s} and $\sqrt{\hat{s}}$ denote the pp and gg (or $b\bar{b}$) c.m.s. energies, respectively, and $dL_{ij}/d\tau$ is the luminosity of colliding partons, which is defined as

$$\frac{dL_{ij}}{d\tau} = \frac{1}{1 + \delta_{ij}} \int_{\tau}^1 \frac{dx_1}{x_1} \left[F_{i/p}(x_1, \mu) F_{j/p}(\frac{\tau}{x_1}, \mu) + (i \leftrightarrow j) \right]. \quad (23)$$

In our calculation we adopt the CTEQ6 parton distribution function [18] and take the factorization scale μ to be $2m_{H^0}$ in the subprocess $gg \rightarrow H^0 H^0$, while μ to be $m_{H^0}/2$ in the calculation of the subprocess $b\bar{b} \rightarrow H^0 H^0$ [19]. The numerical calculation is carried out for the LHC at an energy of 14 TeV.

4 Numerical results and discussions

In the numerical evolution we take the input parameters as $m_W = 80.423$ GeV, $m_Z = 91.1876$ GeV, $m_u = 4.5$ MeV, $m_d = 8.5$ MeV, $m_s = 150$ MeV, $m_c = 1.25$ GeV, $m_t = 174.3$ GeV, and $\alpha(m_Z) = 1/128$. We use a simple one-loop formula to express the running strong coupling constant α_s :

$$\alpha_s(\mu) = \frac{\alpha_s(m_Z)}{1 + \frac{33-2n_f}{6\pi} \alpha_s(m_Z) \ln(\frac{\mu}{m_Z})}, \quad (24)$$

where $\alpha_s(m_Z) = 0.118$ and n_f is the number of active flavors at scale μ [20].

In the numerical calculation, we use the next-to-leading order formula to evaluate the running mass of bottom quark $\overline{m}_b(Q)$ [21].

$$\begin{aligned}\overline{m}_b(Q) &= U_5(Q, \overline{m}_b) \overline{m}_b(\overline{m}_b), & Q < m_t, \\ \overline{m}_b(Q) &= U_6(Q, m_t) U_5(m_t, \overline{m}_b) \overline{m}_b(\overline{m}_b), & Q > m_t,\end{aligned}\tag{25}$$

where $\overline{m}_b = \overline{m}_b(\overline{m}_b) = 4.25$ GeV and the energy scale Q is taken to be $2m_{H^0}$ in our calculation. The evolution factor $U_f(f = 5, 6)$ is

$$\begin{aligned}U_f(Q_2, Q_1) &= \left(\frac{\alpha_s(Q_2)}{\alpha_s(Q_1)} \right)^{d^f} \left[1 + \frac{\alpha_s(Q_1) - \alpha_s(Q_2)}{4\pi} J^f \right], \\ d^f &= \frac{12}{32 - 2f}, \\ J^f &= -\frac{8982 - 504f + 40f^2}{3(33 - 2f)^2}.\end{aligned}\tag{26}$$

In the LH model, the calculation of the Higgs boson pair production at hadron colliders involves four additional free parameters. One is the parameter f , which is the symmetry breaking scale parameter at TeV order. The direct and indirect effects of the LH model provided by the present experimental measurements have placed a constraint $f \gtrsim 3.5$ TeV, although it depends on the model assumption about the $U(1)$'s [17] [22] [23]. The second one is the mass of the Higgs boson, m_{H^0} . The third parameter is the coefficient λ_2 , which is the coupling constant of the new heavy- vector-like quark T . Because there is a relation between the top quark and heavy-vector-like quark coupling parameters λ_1 and λ_2 , as shown in Eq. (14), we can use λ_1/λ_2 to parametrize the mass of the new heavy vector quark [see Eq. (13)]. The last one is v' , and we define $x = 4fv'/v^2$ to parametrize this vacuum expectation value of the scalar triplet field ϕ . The masses of neutral scalar boson

M_{Φ^0} can be given as [16] [17]

$$M_{\Phi^0}^2 = \frac{2m_{H^0}^2 f^2}{v^2[1 - (4v'f/v^2)^2]} = \frac{2m_{H^0}^2 f^2}{v^2(1 - x^2)}. \quad (27)$$

The above equation about the mass of Φ requires a constraint of $0 \leq x < 1$ (i.e., $4v'f/v^2 \lesssim 1$), which shows the relation between the scale f and the vacuum expectation values of the Higgs field doublet and triplet (v, v') . Based on the limitation of current electroweak experimental data [17] [22] [23], in our calculation we choose $f = 3.5$ TeV unless otherwise stated.

Since our numerical calculation shows that the contributions of subprocess $b\bar{b} \rightarrow H^0 H^0$ to the parent process $pp \rightarrow H^0 H^0 + X$ at the LHC is less than 1% of the contributions from subprocess $gg \rightarrow H^0 H^0$, we present only plots of the subprocess $gg \rightarrow H^0 H^0$ for representation. In fact, our analysis also demonstrates that the contributions of the additional diagrams involving the new heavy-vector-like quark T or neutral heavy triplet Higgs boson Φ^0 for the subprocess $gg \rightarrow H^0 H^0$ are very small. The deviations of the cross section from the SM are mainly aroused by the contributions of the diagrams which exist also in the SM, but the interactions between Higgs bosons and quarks in the LH model are different with the corresponding ones in the SM.

The relative effect of the LH on the cross section $[\delta = (\hat{\sigma}_{LH} - \hat{\sigma}_{SM})/\hat{\sigma}_{SM}]$ for subprocess $gg \rightarrow H^0 H^0$ as functions of the c.m.s. energy ($\sqrt{\hat{s}}$) of incoming gluons for the cases of $x = 0$ (corresponding to $M_{\Phi^0} = 3.06$ TeV) and $x = 1/\sqrt{2}$ (corresponding to $M_{\Phi^0} = 4.32$ TeV) are depicted in Fig.3(a), with the parameters taken as $f = 3.5$ TeV and $m_{H^0} = 150$ GeV. In both figures, the solid line, dashed line and dotted line correspond to $\lambda_1/\lambda_2 = 1/2$, $\lambda_1/\lambda_2 = 1$, and $\lambda_1/\lambda_2 = 2$, respectively. From Eq. (12)-(14) we can get that those curves

correspond to $m_T = 6.28$ TeV, 5 TeV, and 6.28 TeV, separately. All the curves in Fig. 3(a) have the common line structure which decreases rapidly in the vicinity of the Higgs boson pair production threshold with an increment of $\sqrt{\hat{s}}$, and then increases steadily after arriving at its minimal value. The curves also obviously show that with an increase of the value of λ_1/λ_2 , the effect of the LH model is getting stronger.

In order to clarify the line shape in Fig. 3(a) more clearly, we present the cross sections in the LH model ($\hat{\sigma}_{LH}$), the SM ($\hat{\sigma}_{SM}$), and the difference between them ($\hat{\sigma}_{LH} - \hat{\sigma}_{SM}$) for the subprocess $gg \rightarrow H^0 H^0$ as functions of $\sqrt{\hat{s}}$ with $m_{H^0} = 150$ GeV, $f = 3.5$ TeV, $\lambda_1/\lambda_2 = 1$, and $x = 0$ in Fig. 3(b) and Table 1. The solid line, dashed line and dotted line in Fig. 3(b) correspond to $\hat{\sigma}_{SM}$, $\hat{\sigma}_{LH}$, and $\hat{\sigma}_{LH} - \hat{\sigma}_{SM}$, respectively. We can see from Fig. 3(b) that in the $\sqrt{\hat{s}}$ region from 310 GeV to 500 GeV the curve for $\hat{\sigma}_{SM}$ rises up steeply, while the $\hat{\sigma}_{LH} - \hat{\sigma}_{SM}$ changes gently, which can be also read from Table 1. Fig. 3(b) and Table.1 show that the polelike behavior of the c.m.s. energy around $\sqrt{\hat{s}} \sim 400\text{-}500$ GeV in Fig. 3(a), comes from the fact that the cross section($\hat{\sigma}_{SM}$) rises up steeply when $\sqrt{\hat{s}}$ is just beyond the threshold energy and decreases gently after $\hat{\sigma}_{SM}$ reaches its maximal value $\sqrt{\hat{s}} \sim 500$ GeV, while the variation of $\hat{\sigma}_{LH} - \hat{\sigma}_{SM}$ is relatively slow in our plotted energy range.

The dependence of the ratio $\hat{\sigma}_{LH}/\hat{\sigma}_{SM}$ of the subprocess $gg \rightarrow H^0 H^0$ on the parameter x with $m_{H^0} = 150$ GeV and $\sqrt{\hat{s}} = 800$ GeV, is depicted in Fig. 4(a). The solid line, dashed line and dotted line correspond to $\lambda_1/\lambda_2 = 1/2$, $\lambda_1/\lambda_2 = 1$, and $\lambda_1/\lambda_2 = 2$, respectively. Fig. 4(a) shows that the effect of the LH model always enhances the cross section of $gg \rightarrow H^0 H^0$ in our chosen parameter space. The three curves also demonstrate that the

$\sqrt{\hat{s}}$	$\hat{\sigma}_{SM}$	$\hat{\sigma}_{LH}$	$\hat{\sigma}_{LH} - \hat{\sigma}_{SM}$	$(\hat{\sigma}_{LH} - \hat{\sigma}_{SM})/\hat{\sigma}_{SM}$
310	0.0052071	0.0060828	0.0008756	0.168162
330	0.0268346	0.0295622	0.0027275	0.101643
350	0.0884609	0.0947308	0.0062699	0.0708781
370	0.2052696	0.2169084	0.0116388	0.0567002
400	0.3425389	0.3595995	0.0170606	0.0498064
420	0.4051675	0.4245253	0.0193578	0.0477772
440	0.4476802	0.4685783	0.0208981	0.0466808
460	0.4738619	0.4957345	0.0218726	0.0461582
490	0.4903020	0.5128817	0.0225796	0.0460525
500	0.4912129	0.5138794	0.0226666	0.0461441
520	0.4880278	0.5107043	0.0226765	0.0464655
540	0.4797802	0.5022973	0.0225171	0.0469321
590	0.4462748	0.4679308	0.0216559	0.048526
700	0.3565471	0.3754663	0.0189191	0.0530621
900	0.2334130	0.2478193	0.0144063	0.06172
1000	0.1935886	0.2063001	0.0127115	0.0656626
2000	0.0598705	0.0659044	0.0060339	0.100783

Table 1: The cross sections of $gg \rightarrow H^0 H^0$ in the LH model and SM, the difference between them, and the relative correction with $m_{H^0} = 150$ GeV, $f = 3.5$ TeV, $\lambda_1/\lambda_2 = 1$, and $x = 1/\sqrt{2}$

effect of the LH model is not sensitive to x in the range of $x \lesssim 0.8$, but their values increase rapidly and can be larger than 1.1 when $x > 0.85$ for all three curves. To explain the result that the correction blows up as we take the $x \rightarrow 1$ limit shown in Fig. 4(a), we decompose the cross sections of subprocess $gg \rightarrow H^0 H^0$ in the LH model into three parts:

$$\hat{\sigma}_{LH} = \hat{\sigma}_{box} + \hat{\sigma}_{tri} + \hat{\sigma}_{int}, \quad (28)$$

where we denote $\hat{\sigma}_{box}$, $\hat{\sigma}_{tri}$, and $\hat{\sigma}_{int}$ as the contribution parts from the box diagrams[including quartic diagrams, shown in Fig. 1(2), 1(3), 1(5), 1(7)], the triangle diagrams[shown in Fig. 1(1), 1(4)] and the interference between the box and triangle diagrams respectively. In Fig. 4(b), we show the contributions of these three parts as functions of x with the conditions

of $\sqrt{s} = 800$ GeV, $m_{H^0} = 150$ GeV, $f = 3.5$ TeV and $\lambda_1/\lambda_2 = 1$. The solid line, dotted line, dash dotted line, and dashed line correspond to box diagrams, triangle diagrams, interference contributions, and total cross section, respectively. Our calculation demonstrates that the main contribution to the cross section of subprocess $gg \rightarrow H^0 H^0$ comes from the box diagrams, and the interference contribution is mainly from the Feynman diagrams involving the top quark. Let us review the couplings of H^0 - H^0 - H^0 and H^0 - \bar{t} - t in the LH model. They can be expressed as

$$g_{H^0 H^0 H^0} : -i \left(\frac{3m_{H^0}^2}{v} - \frac{33m_{H^0}^2 v}{4f^2} \frac{x^2}{1-x^2} \right), \quad (29)$$

$$g_{H^0 \bar{t} t} : -i \frac{m_t}{v} \left[1 + \frac{xv^2}{2f^2} - \frac{x^2 v^2}{4f^2} - \frac{2}{3} \frac{v^2}{f^2} + \frac{v^2}{f^2} \frac{\lambda_1^2}{\lambda_1^2 + \lambda_2^2} \left(1 + \frac{\lambda_1^2}{\lambda_1^2 + \lambda_2^2} \right) \right]. \quad (30)$$

We can see that the contribution of the triangle Feynman diagrams is s -channel suppressed and is relative small, due to the heavy Φ^0 and $\sqrt{s} = 800$ GeV $\gg m_{H^0}$. The figure shows that the contribution from the interference between the box diagrams and triangle diagrams is negative and blows up quickly when we take the $x \rightarrow 1$ limit. We also find that the dependence of the product of $g_{H^0 H^0 H^0}$ and $g_{H^0 \bar{t} t}$ on the parameter x behaves with the same rapid increment when x is close to 1. Therefore, we can conclude that the quick enhancement behavior of the total cross section in the vicinity where $x \rightarrow 1$ arises mainly from contributions of the interference between the triangle diagrams involving the $g_{H^0 H^0 H^0}$ vertex and the box diagrams involving the $g_{h^0 \bar{t} t}$ coupling. As we know, perturbativity alone should put some bounds on the range that x should be allowed to vary. But with these limitations some couplings in the original Higgs potential must behave badly. Since we started with a relatively well-behaved Higgs potential, it is clear that $x \rightarrow 1$ cannot be a

very well-defined limit and should not be considered as a physical limit. In other words, the original Higgs potential is an effective potential result of integrating out the heavy states. Although it cannot give definitive limitations, the size of all Higgs potential parameters should be roughly order 1 theoretically. We depict the relations between x (or g_{HHH}) and the absolute values of original Higgs potential parameters λ_{ϕ^2} , $\lambda_{h\phi h}$, λ_{h^4} , and $\lambda_{h\phi\phi h}$ [see Eq. (10)] in Fig. 4(c) in the conditions of $f = 3.5$ TeV and $m_{H^0} = 150$ GeV. In the figure, the solid line, dashed line, dotted line, and dash-dotted line correspond to $|\lambda_{\phi^2}|$, $|\lambda_{h\phi h}|$, $|\lambda_{h^4}|$, and $|\lambda_{h\phi\phi h}|$, respectively. The absolute value of the coupling $g_{H^0 H^0 H^0}$ corresponding to x value is scaled on the upper axis. From the figure, we can see that the values of all four Higgs potential parameters, which are concerned in our calculation, are far beyond order 1 when $x \gtrsim 0.95$ and $|\lambda_{h\phi\phi h}|$ is less than 10^{-1} when $x \lesssim 0.25$. Therefore, the above x value range should be excluded in our consideration, since these absolute values of the Higgs potential parameters cannot satisfy the request of the well-behaving effective Higgs potential. Then we can approximately put bounds on the varying range of the parameter x as $0.25 < x < 0.95$ on the condition of $f = 3.5$ TeV and $m_{H^0} = 150$ GeV.

The ratio of total cross sections σ_{LH}/σ_{SM} , as functions of x at the LHC ($\sqrt{s} = 14$ TeV) with $f = 3.5$ TeV and $\lambda_1/\lambda_2 = 2$ is depicted in Fig. 5. The total cross section involves the contributions of both subprocesses $gg \rightarrow H^0 H^0$ and $b\bar{b} \rightarrow H^0 H^0$. In the figure, the solid line, dashed line, and dotted line correspond to $m_{H^0} = 115$ GeV, 150 GeV, and 180 GeV, respectively. We can see again that the deviation of the total cross section in the LH model from the corresponding SM value is not sensitive to x when $x \lesssim 0.8$, but increases quickly when $x > 0.9$, and the relative deviation, defined as $\delta = (\sigma_{LH} - \sigma_{SM})/\sigma_{SM}$, can be

beyond 12% when x reach 0.9 at the LHC. We can see from this figure that the correction effect of the LH model is obviously related to the Higgs boson mass. When the Higgs boson mass varies in the range of 115 – 180 GeV, the curves show that the heavier the Higgs boson mass is, the stronger the correction effect becomes.

In Fig. 6 we plot the ratio between the total cross sections in the LH model and the SM, as the functions of the mass of the neutral Higgs boson m_{H^0} with the conditions of $f = 3.5$ TeV and $\lambda_1/\lambda_2 = 2$ at the LHC. In this figure, the solid line, dashed line, and dotted line correspond to the cases of $x = 0.25$, $1/\sqrt{2}$ and 0.9 respectively. The relative correction of the LH model to the SM cross section [$\delta = (\sigma_{LH} - \sigma_{SM})/\sigma_{SM}$], can reach 14.8% when $x = 0.9$ at the LHC.

The total cross sections σ_{SM} and σ_{LH} of process $pp \rightarrow H^0 H^0$ as functions of the mass of the neutral Higgs boson m_{H^0} is depicted in Fig. 7 at the LHC, with $f = 3.5$ TeV, $x = 0.9$, and $\lambda_1/\lambda_2 = 2$ in the LH model. The solid line and dashed line correspond to the cases of the SM and LH model, respectively. They show that the absolute correction induced by the LH model decreases with an increase of the Higgs boson mass.

In Fig. 8, we plot the total cross sections σ_{LH} of process $pp \rightarrow H^0 H^0$ as functions of the new heavy vector-like quark mass m_T with $m_{H^0} = 150$ GeV and $x = 1/\sqrt{2}$ in the LH model at the LHC. In this figure the solid line is for $\lambda_1/\lambda_2 = 1/2$, dashed line for $\lambda_1/\lambda_2 = 1$, and dotted line for $\lambda_1/\lambda_2 = 2$. According to Eq. (13) for a fixed value of λ_1/λ_2 , the mass of heavy-vector-like quark T is only related to the symmetry breaking scale parameter f . For example, when $\lambda_1/\lambda_2 = 2$ and m_T varies from 1.5 TeV to 4.0 TeV, we have that the parameter f changes from 0.85 TeV to 2.26 TeV. We can see from this

figure that in the chosen parameter space the cross sections are enhanced when either m_T is relatively small or λ_1/λ_2 is relatively larger.

In conclusion, we investigated the effect of the LH model on the pair production process of neutral Higgs bosons via both gluon and bottom fusions at the LHC. The numerical analysis shows that with the possible parameters, the relative cross section correction to the SM prediction may reach a value of 24% at the LHC when $x = 0.95$. We conclude that when the parameter x has a value above 0.8, the relative correction contributed by the LH model reached a value beyond 8% and could be observable at the LHC.

Acknowledgement: This work was supported in part by the National Natural Science Foundation of China and a grant from the University of Science and Technology of China.

Appendix

The interactive Lagrangian of the scalar field Σ and the up-type quarks of the first two generations take the same form as in Eq. (11), except that there is no need for the extra \tilde{t} . The interactive Lagrangian of the Σ and the down-type quarks can be expressed as

$$\mathcal{L}_Y = \frac{1}{2} \lambda_d f \epsilon_{ijk} \epsilon_{xy} \chi_i \Sigma_{jx}^* \Sigma_{ky}^* d^c + H.C., \quad (31)$$

where the isospin index $i = 1, 2$. All the Yukawa couplings between the Higgs boson and quarks (except the Yukawa coupling which involves the top quark) can be obtained from the corresponding Lagrangian directly. We present the expressions of the H^0 - H^0 - \bar{u} - u and H^0 - H^0 - \bar{d} - d couplings in the equations

$$g_{H^0 H^0 \bar{d} d} : -i \frac{4m_d v'}{v^2(f + v')} \quad , \quad g_{H^0 H^0 \bar{u} u} : -i \frac{4m_u v'}{v^2(f + v')} . \quad (32)$$

The expressions of other couplings concerned with in this work can be found in Ref. [17].

In the LH model, the trilinear interaction of Higgs bosons $g_{H^0 H^0 H^0}$ gets a correction to the SM at the order of v^2/f^2 , and an additional $H^0 H^0 \Phi^0$ coupling is generated. They are given by the Lagrangians

$$\begin{aligned} -\mathcal{L}_{HHH} &= H^0 H^0 H^0 \left(-\frac{2fv'\lambda_{h\phi h}}{v} + v\lambda_{h^4} - \frac{12v'^2\lambda_{h^4}}{v} + \frac{6v'^2\lambda_{h\phi\phi h}}{v} \right), \\ -\mathcal{L}_{HH\phi} &= H^0 H^0 \phi^0 \left(-\frac{f\lambda_{h\phi h}}{\sqrt{2}} + \frac{14\sqrt{2}fv'^2\lambda_{h\phi h}}{v^2} - 6\sqrt{2}v'\lambda_{h^4} + \frac{5v'\lambda_{h\phi\phi h}}{\sqrt{2}} \right). \end{aligned} \quad (33)$$

From the above Lagrangians we obtain the Feynman rule for $H^0 H^0 H^0$ and $H^0 H^0 \Phi^0$ couplings as [17]

$$\begin{aligned} g_{H^0 H^0 H^0} &: -i \left(\frac{3m_{H^0}^2}{v} - \frac{66M_{\Phi^0}^2 v'^2}{f^2 v} \right), \\ g_{H^0 H^0 \phi^0} &: -i \left(\frac{56\sqrt{2}M_{\Phi^0}^2 v'^3}{v^4} - \frac{2\sqrt{2}M_{\Phi^0}^2 v'}{v^2} - \frac{29\sqrt{2}M_{\Phi^0}^2 v'}{3f^2} \right). \end{aligned} \quad (34)$$

References

- [1] S. L. Glashow, Nucl. Phys. **22**, 579 (1961) ; S. Weinberg, Phys. Rev. Lett. **1**, 1264 (1967); A. Salam, in *Proceedings of the 8th Nobel Symposium*, Stockholm, 1968, edited by N. Svartholm (Almqvist and Wiksells, Stockholm, 1968), p.367; H. D. Politzer, Phys. Rep. **14** 129 (1974).
- [2] P. W. Higgs, Phys. Lett **12**, 132 (1964), Phys. Rev. Lett. **13**, 508 (1964); Phys. Rev. **145**, 1156 (1966); F. Englert and R. Brout, Phys. Rev. Lett. **13**, 321 (1964); G. S. Guralnik, C. R. Hagen, and T. W. B. Kibble, *ibid.* **13**, 585 (1964); T. W. B. Kibble, Phys. Rev. **155**, 1554 (1967).

- [3] N. Arkani-hamed, A. G. Cohen and H. Georgi, Phys. Lett. B **513**, 232 (2001).
- [4] N. Arkani-hamed, A. G. Cohen, T. Gregoire, and J. G.Jacker, J. High Energy Phys. **08**, 020 (2002).
- [5] N. Arkani-hamed, A. G. Cohen, E. Katz, A. E. Nelson, T. Gregoire and J. G. Wacker, J. High Energy Phys. **08**, 021 (2002) .
- [6] I. Low, W. Skiba and D.Smith, Phys. Rev. D **66**, 072001 (2002).
- [7] N. Arkani-hamed, A. G. Cohen, E. Katz and A. E. Nelson, J. High Energy Phys. **07**, 304 (2002).
- [8] For a recent review, see e.g., M. Schmaltz, Nucl. Phys. B (Proc. Suppl.) **117**, 40 (2003).
- [9] T. Gregoire and J. G. Wacker, J. High Energy Phys. **08**, 019 (2002).
- [10] S. Dawson, S. Dittmaier, and M. Spira, Phys. Rev. D **58**, 40 (1998).
- [11] E.W.N. Glover and J.J. van der Bij, Nucl. Phys. **B309**, 282 (1988)
- [12] A. Krause, T. Plehn, M. Spira, P.M. Zerwas, Nucl.Phys. **B519**, 85 (1998); T. Plehn, M. Spira, P.M. Zerwas, Nucl.Phys. **B479**, 46 (1996); Jiang Yi, Han Liang, Ma Wen-Gan, Yu Zeng-Hui and Han Meng, J. Phys. **G23**, 385 (1997); J. Phys. **G23**, 1151 (1997).
- [13] A.A. Barrientos Bendezu and B.A. Kniehl, Phys. Rev. **D64**, 035006 (2001)
- [14] U. Baur, T. Plehn and D. Tainwater, Phys. Rev. Lett. **89**, 151801 (2002).

- [15] C. Dib, R. Rosenfeld and A. Zerwekh, "Higgs Production and decay in the little Higgs Model",
[`\protect\vrule width0pt\protect\href{http://arxiv.org/abs/hep-ph/0302068}`]{hep-ph/0302068}
- [16] T. Han, H. E. Logan, B.McElrath and L. T. Wang , Phys. Lett. B **563**, 191 (2003).
- [17] T. Han, H. E. Logan, B.McElrath and L.T. Wang, Phy. Rev. D **67**, 095004 (2003).
- [18] H. L. Lai,J. Huston, and S. Kuhlmann, Eur. Phys. J. C **12**, 375 (2000).
- [19] F. Maltoni, Z. Sullivan, and S. Willenbrock, Phys. Rev. D **67**, 093005 (2003).
- [20] K.Hagiwara *et al.*, Phys. Rev. D **66**, 010001 (2002).
- [21] M. Carena, D. Garcia, U. Nierste and C.E.M. Wagner, Nucl. Phys. **B577**, 88 (2000).
- [22] C. Csaki, J. HUBisz, G. D. Kribs and P. Meade, and J. Terning, Phys. Rev. D **67**, 115002 (2003); Phys. Rev. D **68**, 035009 (2003).
- [23] J. L. Hewett, F. J. Petriello and T. G. Rizzo, J. High Energy Phys. **10**, 062 (2003);
S. Chang and Hong-Jian He, Phys. Lett. B **586**, 95 (2004)

Figure Captions

Fig. 1 The one-loop Feynman diagrams of the subprocess $gg \rightarrow H^0 H^0$ in the LH model: (1), (4) s -channel diagrams. (2), (3), (5), (6) box diagrams. (7) quartic diagrams. The notations u and d represent up-type and down-type quarks, respectively. The dia-

grams created by exchanging two external gluon lines and final Higgs boson lines are not shown.

Fig. 2 The lowest-order Feynman diagrams of the subprocess $b\bar{b} \rightarrow H^0 H^0$ in the LH model.

Fig.3(a) The relative effect of the LH on the cross section $[\delta = (\hat{\sigma}_{LH} - \hat{\sigma}_{SM})/\hat{\sigma}_{SM}]$ for subprocess $gg \rightarrow H^0 H^0$ as functions of $\sqrt{\hat{s}}$ on the conditions of $x = 1/\sqrt{2}, f = 3.5$ TeV, $m_{H^0} = 150$ GeV. The solid line, dashed line, and dotted line correspond to $\lambda_1/\lambda_2 = 1/2$, $\lambda_1/\lambda_2 = 1$, and $\lambda_1/\lambda_2 = 2$, respectively. **(b)** The cross sections of $gg \rightarrow H^0 H^0$ subprocess in the SM, the LH model, and their difference $\hat{\sigma}_{LH} - \hat{\sigma}_{SM}$ as functions of $\sqrt{\hat{s}}$ with $x = 1/\sqrt{2}$, $f = 3.5$ TeV, $m_{H^0} = 150$ GeV, and $\lambda_1/\lambda_2 = 1$.

Fig. 4(a) The dependence of the ratio $\hat{\sigma}_{LH}/\hat{\sigma}_{SM}$ for the subprocess $gg \rightarrow H^0 H^0$ on the parameter x with $m_{H^0} = 150$ GeV and $\sqrt{\hat{s}} = 800$ GeV. The solid line, dashed line and dotted line correspond to $\lambda_1/\lambda_2 = 1/2$, $\lambda_1/\lambda_2 = 1$, and $\lambda_1/\lambda_2 = 2$, respectively. **(b)** The total cross section and contributions of the box diagrams (including quartic diagrams), the triangle diagrams, interference between the box and triangle diagrams ($\hat{\sigma}_{LH} = \hat{\sigma}_{box} + \hat{\sigma}_{tri} + \hat{\sigma}_{int}$) for the subprocess $gg \rightarrow H^0 H^0$, as functions of x with the conditions of $\sqrt{\hat{s}} = 800$ GeV, $m_{H^0} = 150$ GeV, $f = 3.5$ TeV, and $\lambda_1/\lambda_2 = 1$. The solid line, dotted line, dash dotted line, and dashed line correspond to box diagrams, triangle diagrams, interference contributions, and total cross section respectively. **(c)** The absolute value of the original Higgs potential parameters λ_{ϕ^2} , $\lambda_{h\phi h}$, λ_{h^4} and $\lambda_{h\phi\phi h}$ as functions of x with the conditions of $m_{H^0} = 150$ GeV and $f = 3.5$ TeV. The absolute value of coupling $g_{H^0 H^0 H^0}$ corresponding to the x value is scaled on the upper axis.

Fig. 5 The ratio of the total cross sections in the LH model and SM σ_{LH}/σ_{SM} for the process $pp \rightarrow H^0 H^0$ at the LHC, as functions of x ($= 4fv'/v^2$), with $f = 3.5$ TeV and $\lambda_1/\lambda_2 = 2$.

Fig. 6 The ratio of the total cross sections σ_{LH}/σ_{SM} for the process $pp \rightarrow H^0 H^0$ at LHC, as functions of the Higgs boson mass m_{H^0} with the conditions of $f = 3.5$ TeV and $\lambda_1/\lambda_2 = 2$ in the LH model.

Fig.7 The total cross sections σ_{SM} and σ_{LH} for the process $pp \rightarrow H^0 H^0$ at the LHC, as functions of the Higgs boson mass m_{H^0} with $f = 3.5$ TeV, $x = 0.9$ and $\lambda_1/\lambda_2 = 2$.

Fig.8 The total cross section σ_{LH} as functions of the mass of the new heavy-vector-like quark m_T with $m_{H^0} = 150$ GeV and $x = 1/\sqrt{2}$ in the LH model at the LHC.

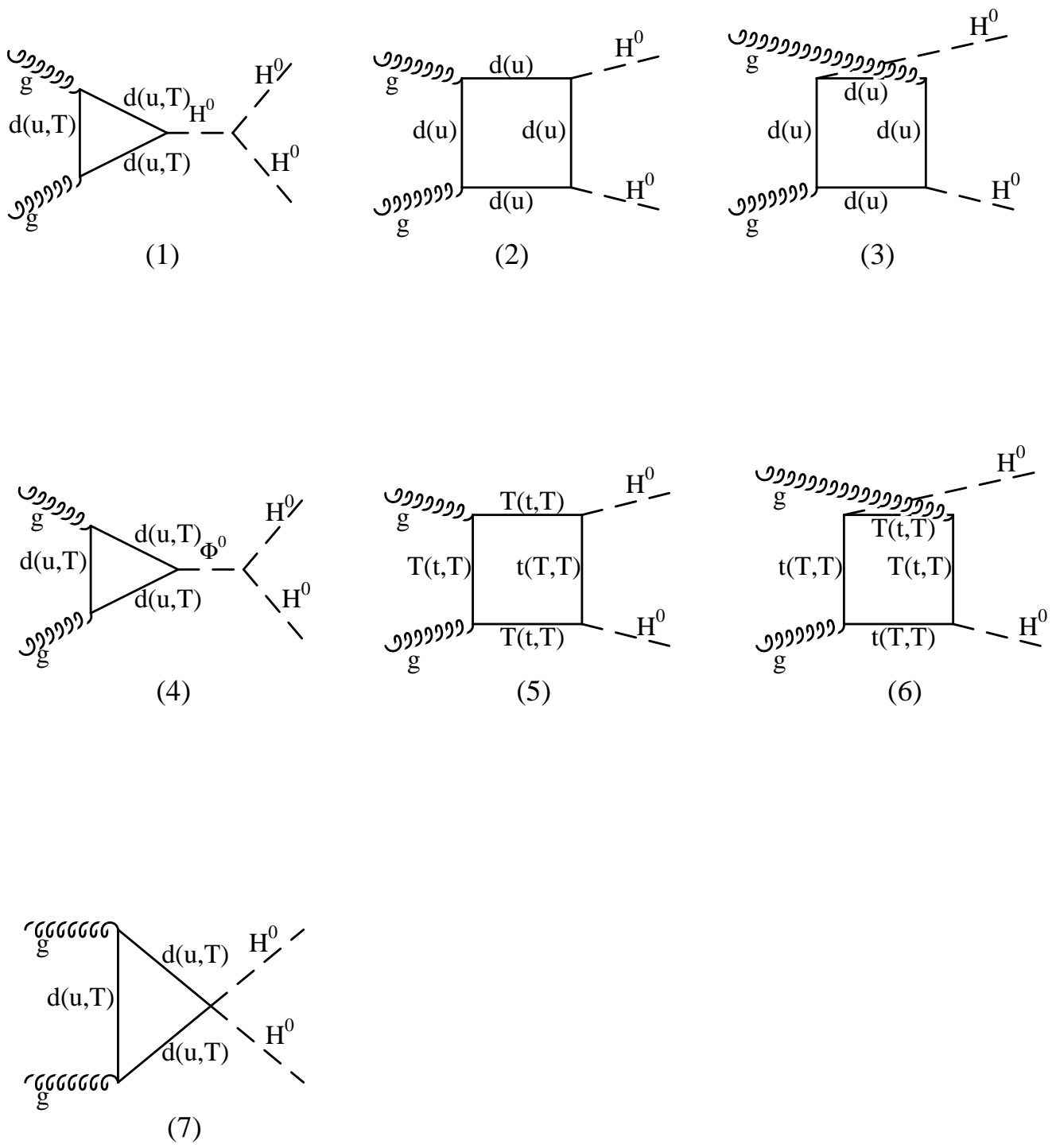


Fig.1

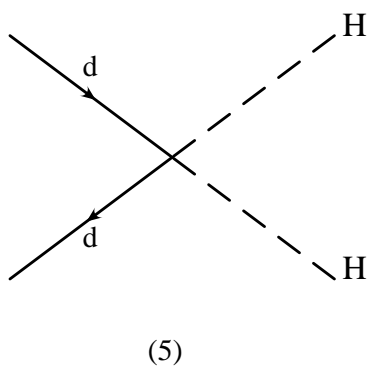
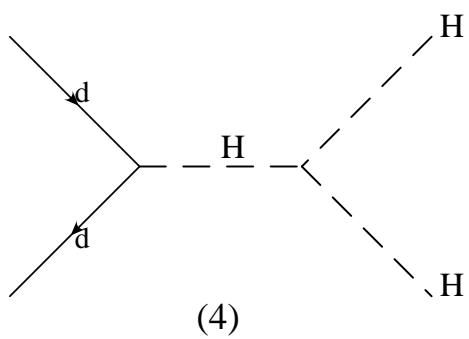
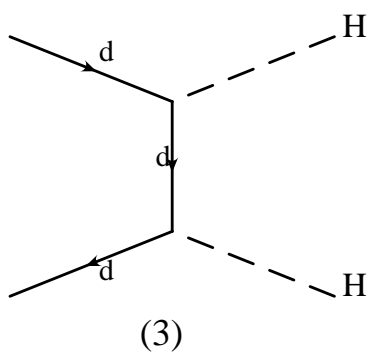
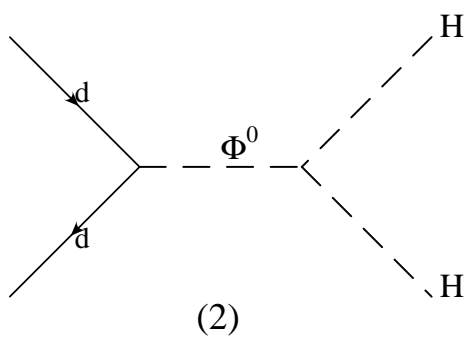
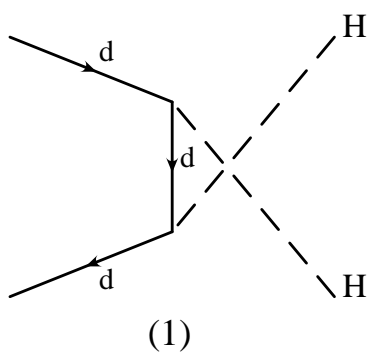


Fig.2

Fig .3(a)

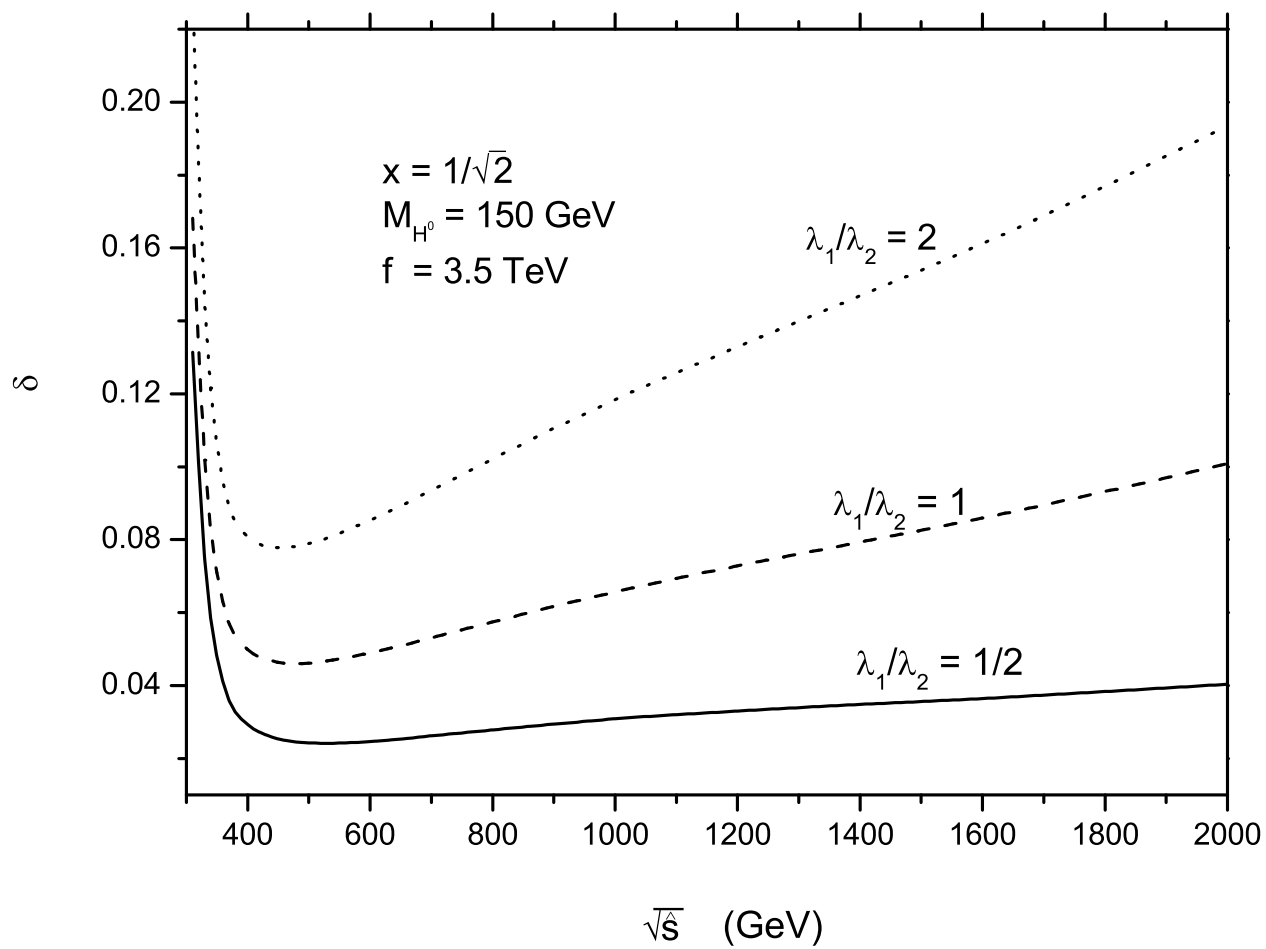


Fig . 3(b)

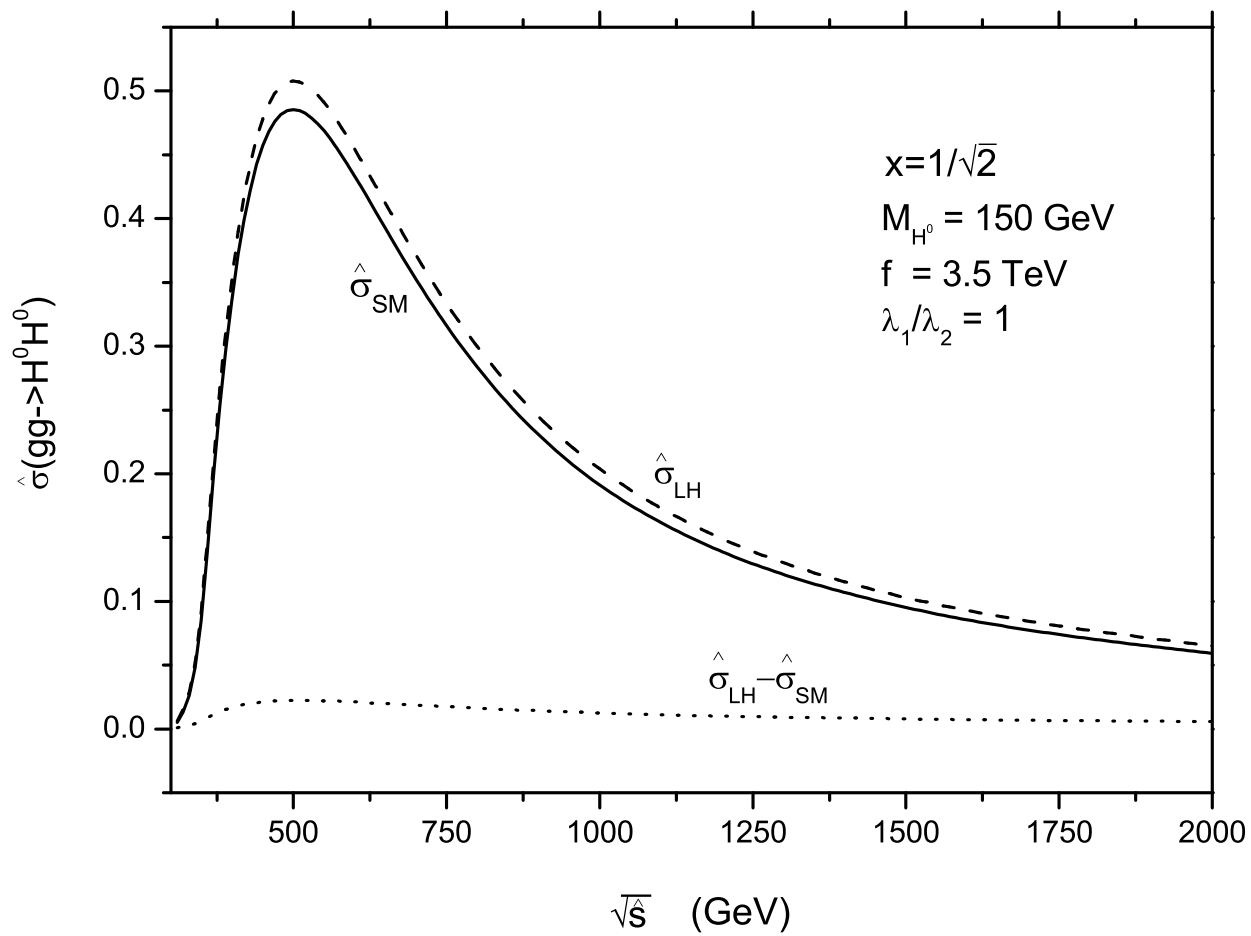


Fig . 4(a)

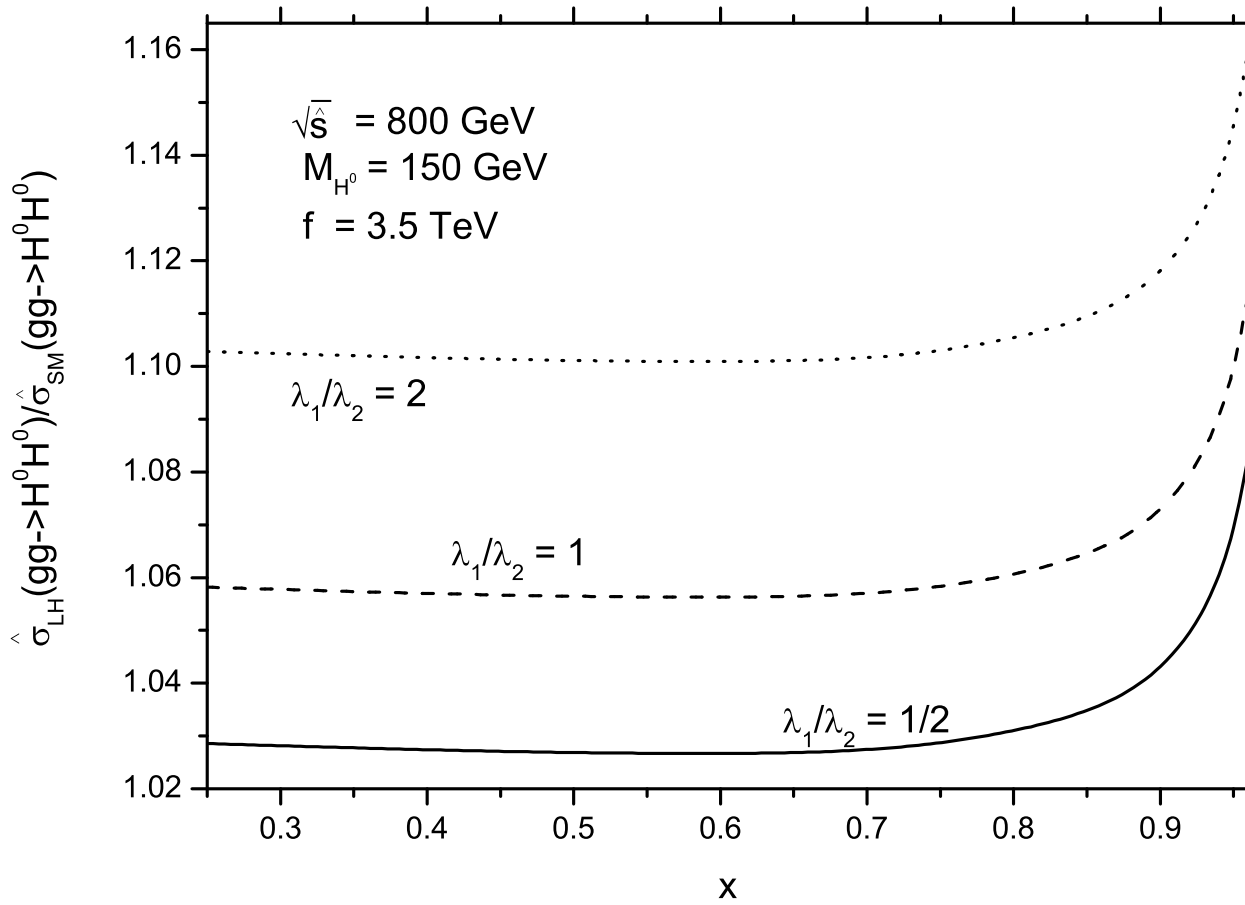


Fig . 4(b)

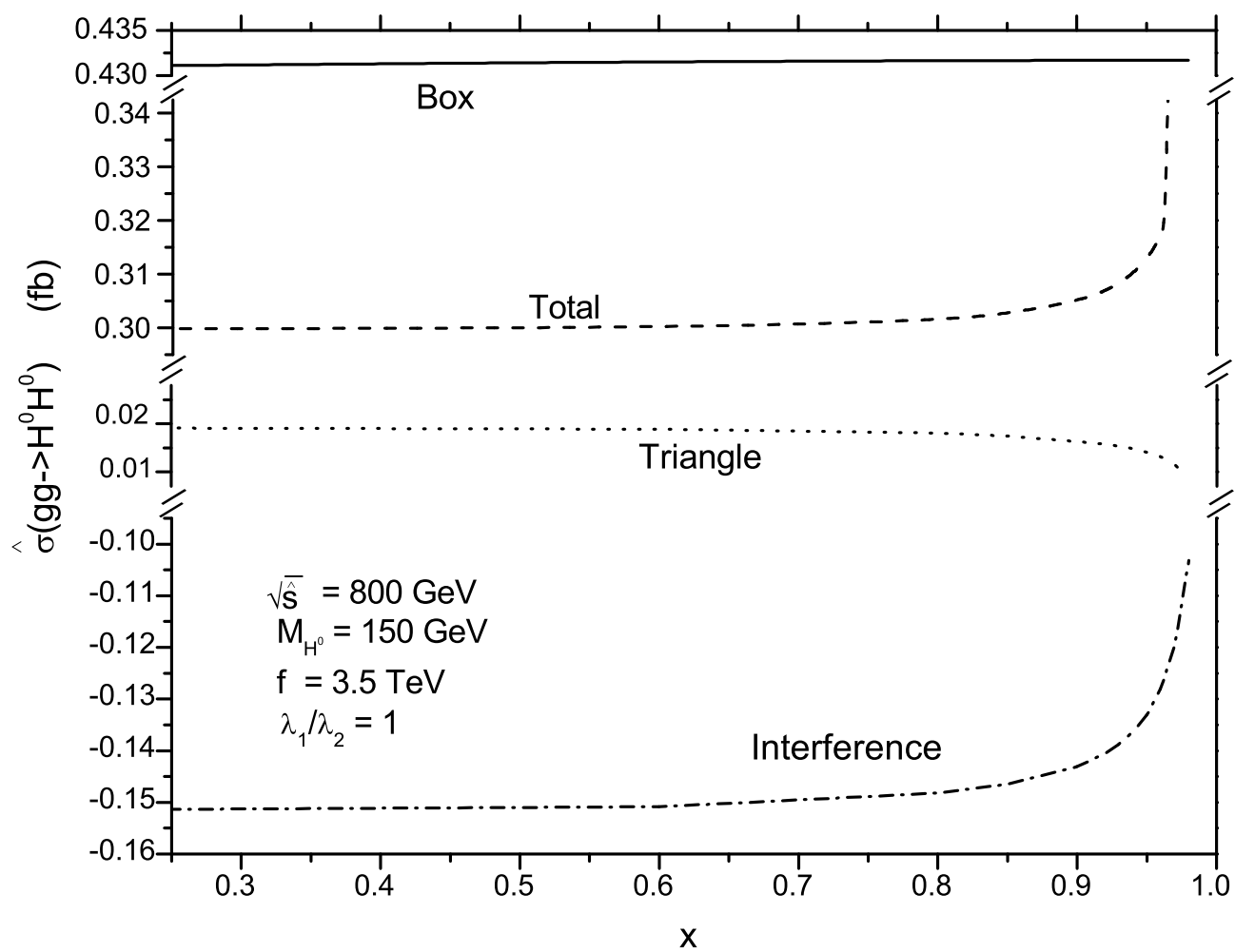


Fig. 4(c)

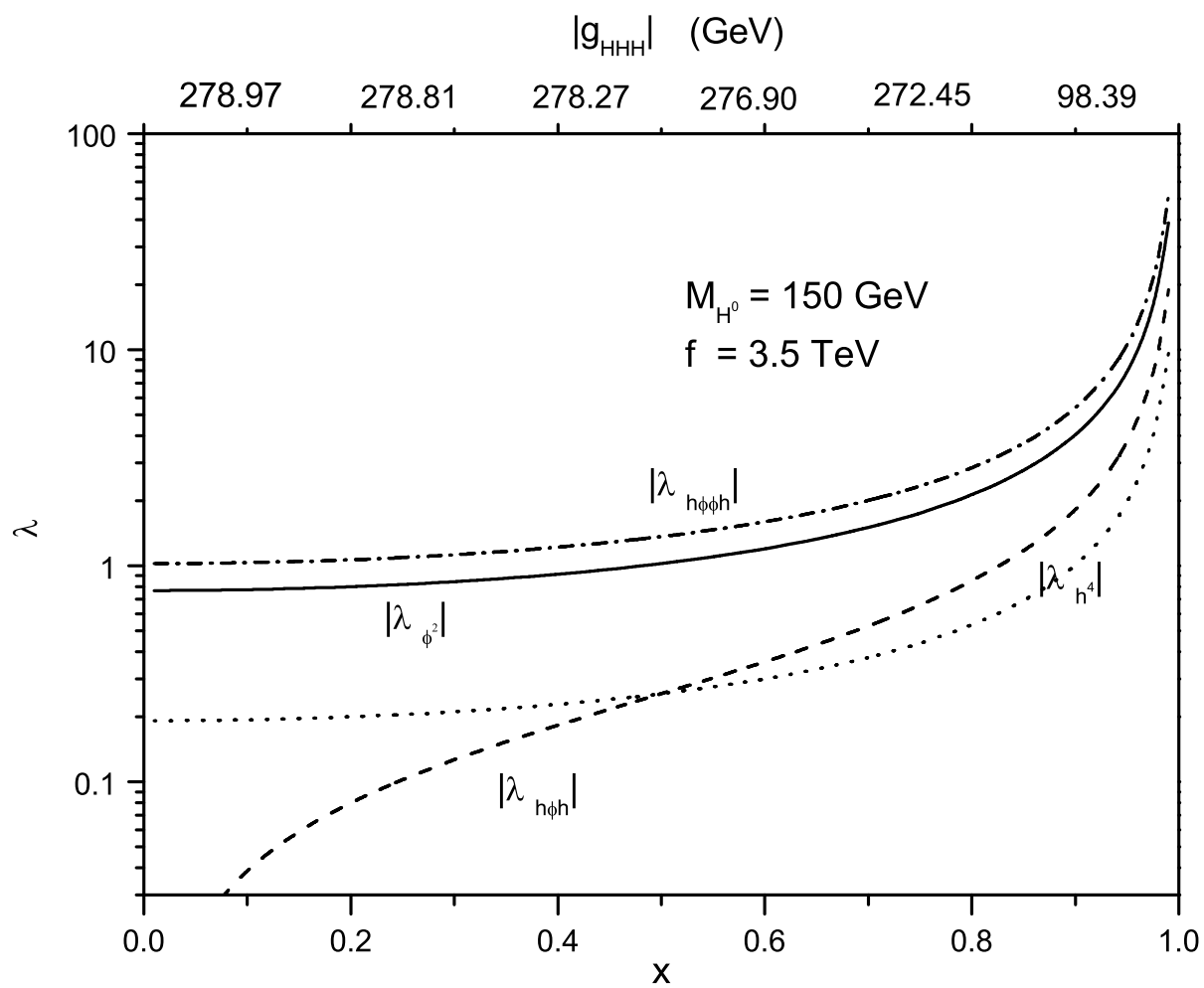


Fig . 5

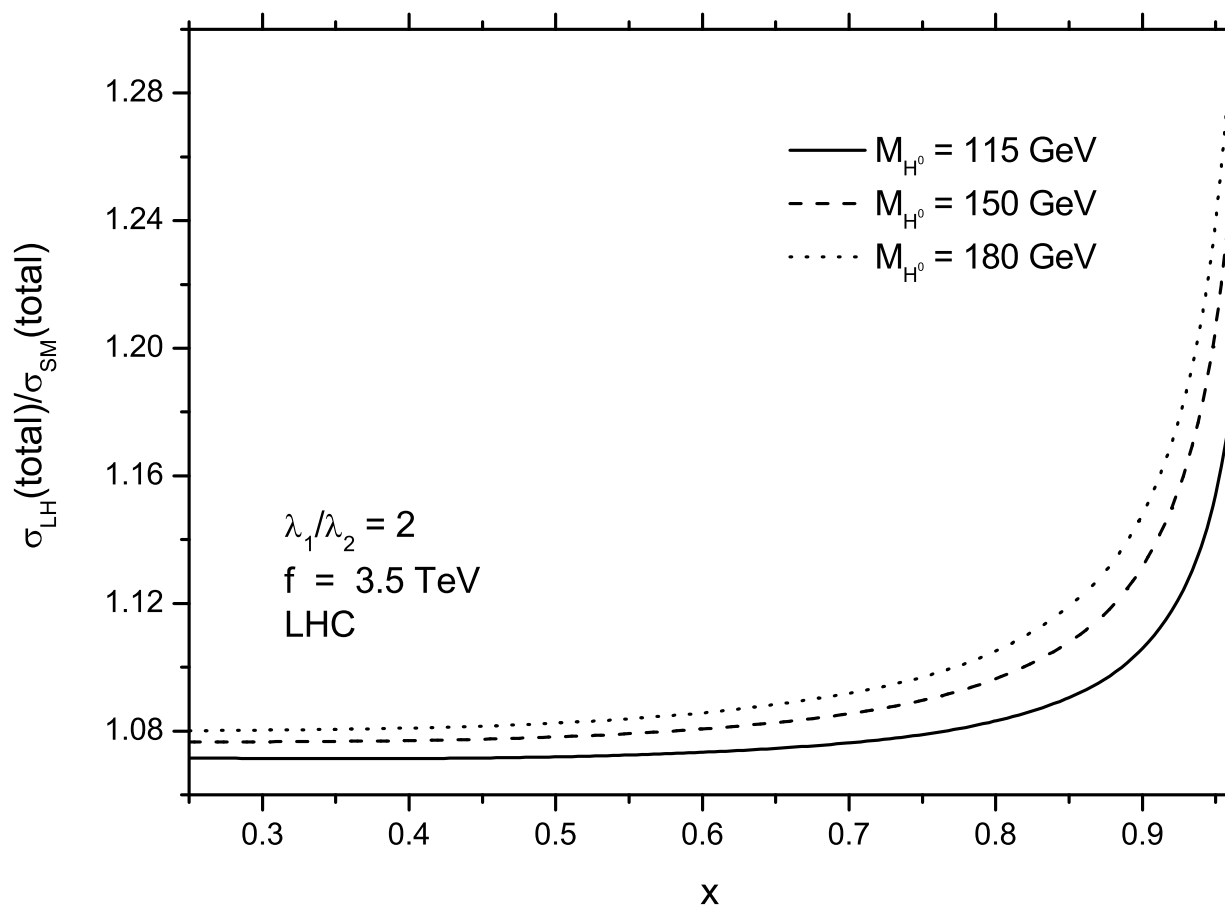


Fig . 6

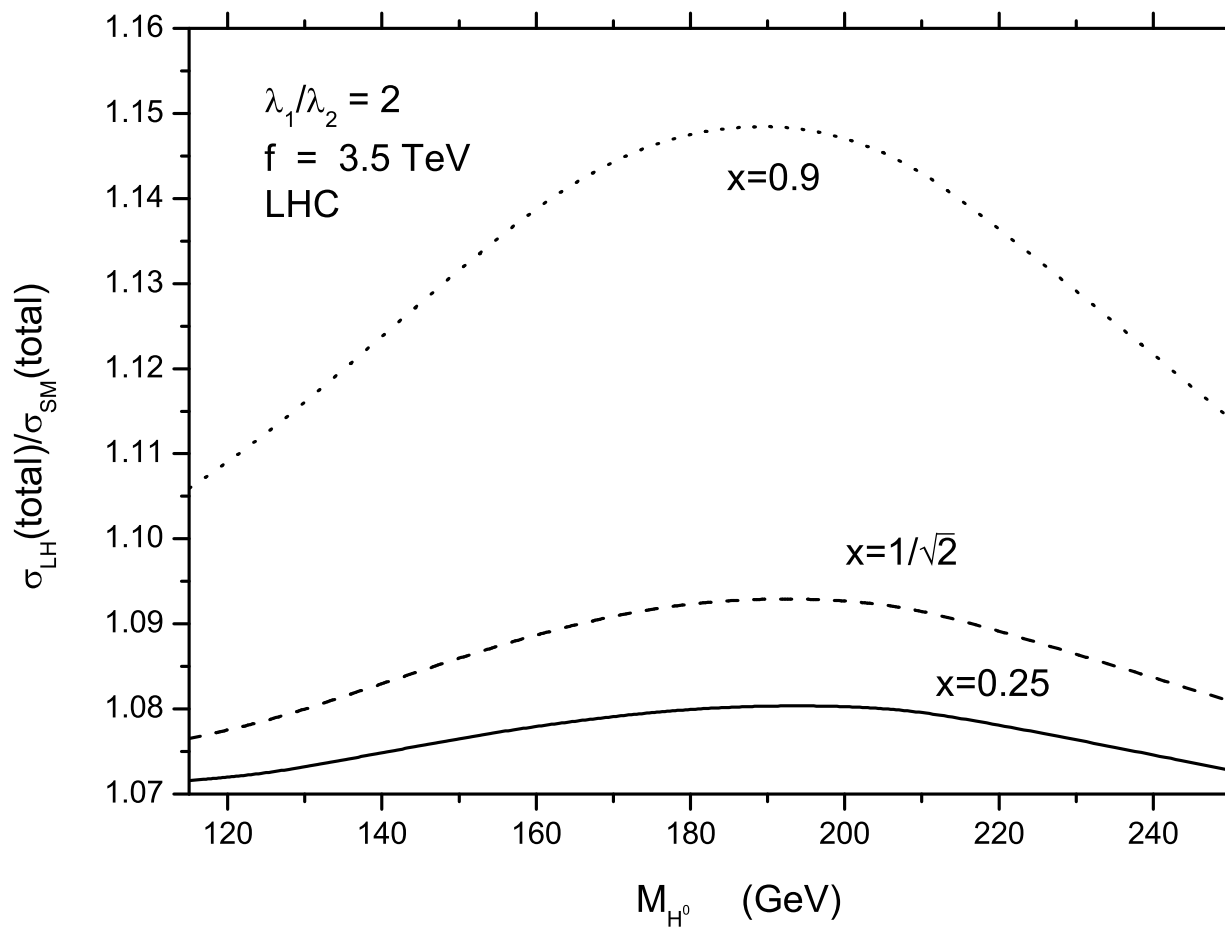


Fig . 7

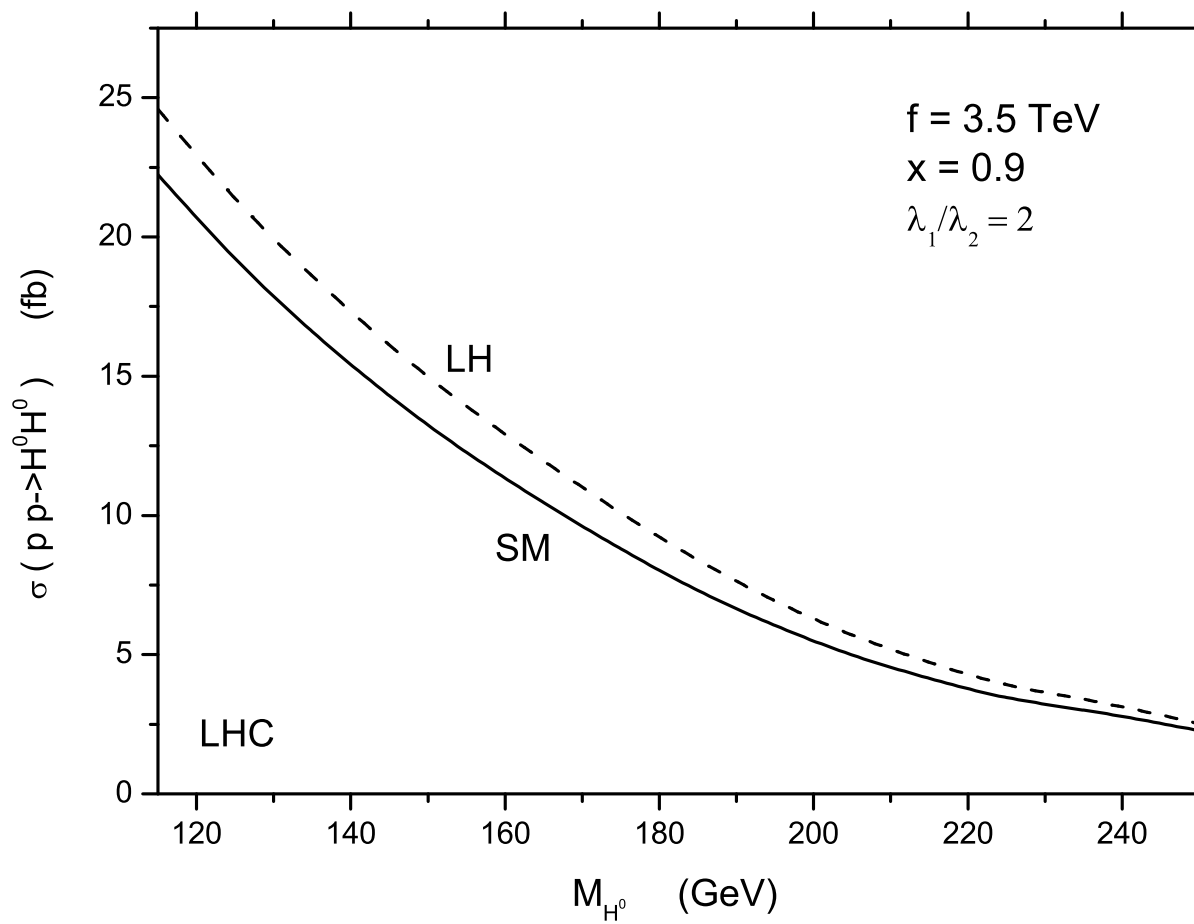


Fig . 8

